Sub-millisecond phase contrast wavefront sensor based on an optically addressed ferroelectric liquid crystal spatial light modulator

Leonid Beresnev, Mikhail Vorontsov, and John Gowens

Army Research Laboratory, Intelligent Optics Lab, 2800 Powder Mill Road, Adelphi MD, 20783.
Phone: (301)394-0213, (301)394-0214, fax (301)394-0225, e-mail address: beresnev@iol.arl.army.mil, mvorontsov@arl.army.mil

ABSTRACT

A sub-millisecond wavefront sensor based on a non-linear Zernike filter is described. The sensor's key element is an optically addressed spatial light modulator (OASLM). The OASLM is composed of ferroelectric liquid crystal and an amorphous silicon carbide photo-conducting film. The OASLM is placed into the focal plane of a Fourier filtering system. The sensor operates with circularly polarized input light. For the high intensity (zero order) spectral component the deviation of the ferroelectric liquid crystal director by $\pi/4$ (45^o) results in a $\pi/2$ phase shift. This provides wavefront phase distortion visualization similar to a conventional Zernike filter. The registered characteristic response time of the sensor is near 0.2ms for light intensity on the order of 100nW.

Keywords: wave front sensor, optically addressed spatial light modulator, ferroelectric liquid crystal

1. INTRODUCTION

The operation rate of existing wavefront sensors is dependent on the sensor resolution and typically decreases with an increase in resolution. However, the upcoming new wavefront phase correcting devices with a high number of elements on the order of $10^4...10^6$ require both high resolution and high operational speed. It is difficult to fulfill such demand utilizing traditional wavefront sensors used in adaptive optics: shearing interferometers, Shack-Hartmann sensors, curvature sensors, etc. In these sensors, the wavefront phase is reconstructed from its first or second derivatives, which requires extensive calculations resulting in a relatively low operation rate [1-5].

Time-consuming calculations are also the principle obstacle for wavefront sensors based on focal plane techniques: phase retrieval from a set of pupil and focal plane intensity distributions, phase diversity, or Schlieren techniques [6-13]. For these methods, the dependence of the wavefront sensor output intensity (sensor output image) on phase is nonlinear, and phase reconstruction requires the solution of rather complicated inverse problems.

The phase-contrast technique invented by F. Zernike (Zernike filter shown in Fig. 1) offers a simple wavefront sensor configuration that can provide both high-resolution and high-speed wavefront visualization of phase distortions in the absence of large amplitude wavefront tilts. The Zernike filter consists of a glass slide with a fixed phase-shifting dot placed in the focal plane of lens. This phase-shifting dot is used to provide phase-shift by $\pi/2$ of the zero-order spectral component of a monochromatic input wave [12-14].

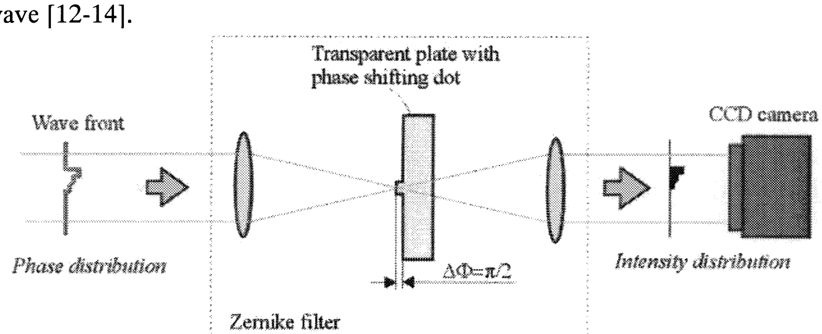

Fig.1. Phase-contrast Zernike filter for transformation of wavefront phase distribution to an intensity distribution.

High-Resolution Wavefront Control: Methods, Devices, and Applications III, John D. Gonglewski, Mikhail A. Vorontsov, Mark T. Gruneisen, Editors, Proceedings of SPIE Vol. 4493 (2002)

The primary limitation of the Zernike filter is its lack of robustness to optical component misalignment and to wavefront tilts.

In [15,16] we have proposed and experimentally demonstrated a wavefront sensor based on an optically addressed spatial light modulator (OASLM) that can generate a self-adjusting phase-shifting dot that coincides with the location of the most intensive (zero) spectral component. This dot is created due to reorientation of the nematic liquid crystal layer embedded between two transparent ITO (indium tin oxide) electrodes. One electrode contains deposited photo-conducting film semi-transparent for input light. This wavefront sensor is shown in Fig. 2.

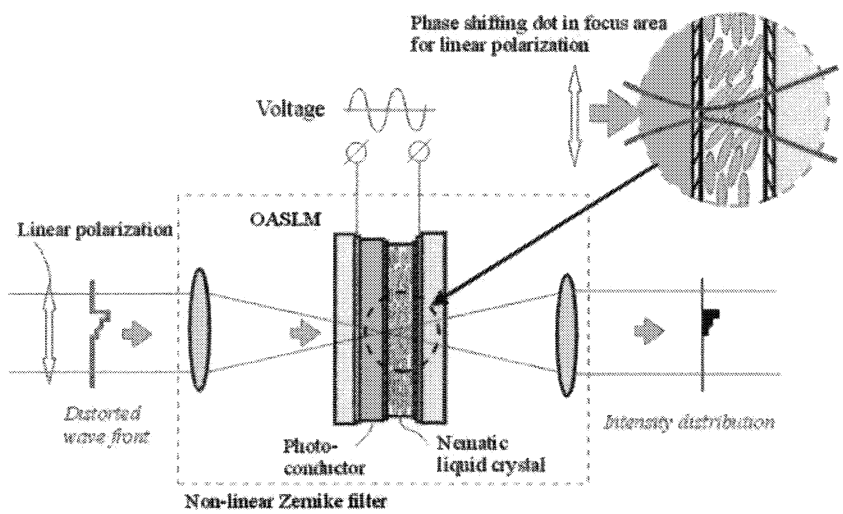

Fig.2. Non-linear Zernike filter based on optically addressed spatially light modulator, using nematic liquid crystal.

In an area of the LC OASLM where light intensity level is small the LC layer is uniformly aligned. This leads to uniform retardation of the wavefront equal to $n_{II}d$, where n_{II} is the refractive index along the nematic liquid crystal director (direction of long axes of LC molecules), d is the thickness of the liquid crystal layer.

At the area of relatively high light intensity the conductivity of the photo-conducting film increases resulting in a non-uniform decrease of the wavefront retardation. The highest reorientation of liquid crystal molecules from a planar to homeotropic state takes place in the area corresponding to the zero spatial spectral component. At an appropriate intensity and applied OASLM voltage an optical retardation phase shift of $\pi/2$ can be achieved. The sensitivity of the described non-linear Zernike filter [15] based on nematic OASLM was on the order of microWatts with a response time on the order of 10ms. The characteristic operational rate of this device was near 50Hz.

In this paper we introduce a non-linear Zernike filter using ferroelectric liquid crystal (FLC) optically addressed spatial light modulator as shown in Fig.3. Optical states of ferroelectric liquid crystal layer in OASLM are shown in Fig. 4.

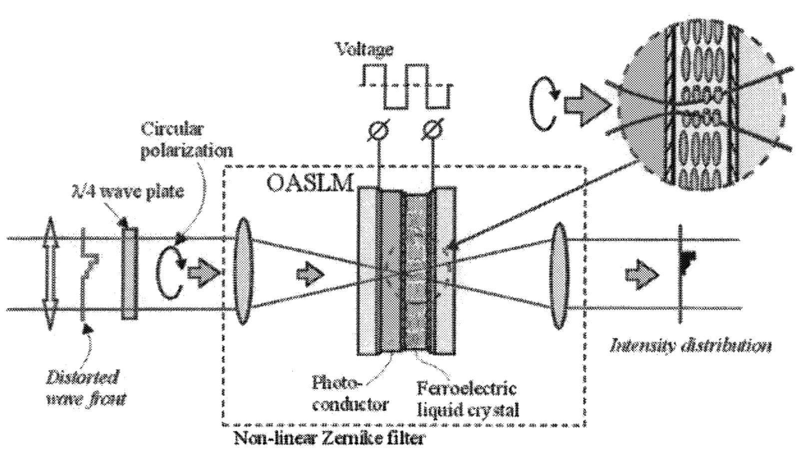

Fig.3. Non-linear Zernike filter based on optically addressed ferroelectric liquid crystal spatial light modulator.

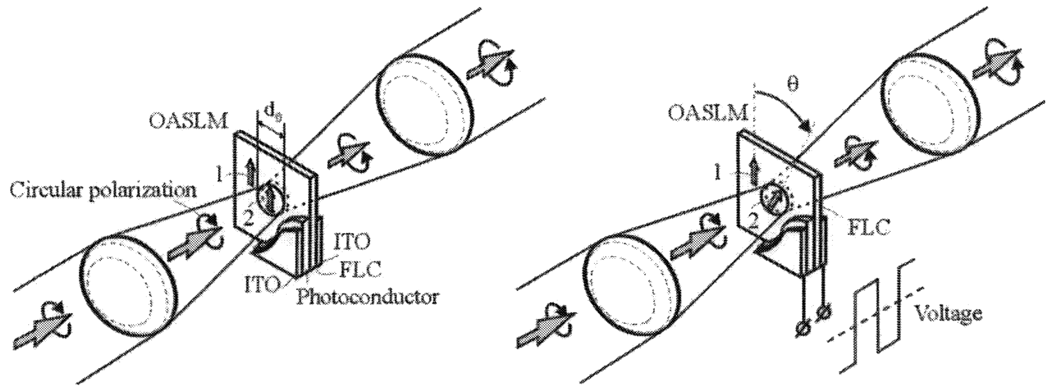

a b

Fig. 4. Optical states of FLC layer of OASLM: a) no voltage applied; b) voltage is applied to OASLM. The additional optical phase shift $\Delta\Phi = 2\Theta$ for circular polarization of input light beam takes place in the focus area 2 with diameter d_o, corresponding to zero spatial component, relative to ambient area 1 of OASLM. (Θ is dependent on intensity angle of deviation of FLC optical axes).

A linear polarizer and quarter wave plate in Fig.3 are used to obtain circular polarization of light coming onto the OASLM. The zero spatial frequency component of the input beam focused on the OASLM produces a spot with diameter $d_o = f\lambda/D$. With a Fourier lens having a focal length f=30cm and aperture D = 15mm (wavelength λ = 633nm), the diameter d_o = 10μm. In the case of high enough intensity local re-orientation of the liquid crystal molecules occurs only in the zero spectral component area as shown in Fig.4b. Assume that the FLC layer thickness d satisfies to the condition $d\Delta n = \lambda/2 + N\lambda$, where Δn is optical anisotropy of the FLC material ($\Delta n = n_{II} - n_{\perp}$, n_{II} and $n_{\perp}$ are refractive indices along and perpendicular to FLC director), and N is an integer.

After passing through the FLC layer the output wave is still circular polarized, but the polarization handedness sign is changed. In addition in the area of zero order spectral component the phase shift

$$\Delta\Phi = 2\Theta, \qquad (1)$$

occurs. This phase shift is proportional to deviation in the angle Θ between directors of the FLC in the area of zero spectral component and in ambient area. Relationship (1) is a characteristic property of uni-axial plate with retardation $\lambda/2$, placed into the beam with circular polarization [17].

To provide optical phase shift of circular polarized light different FLC types can be used. Among them are surface stabilized FLC (SSFLC) [18], electroclinic materials [19], helical smectic materials with deformed helix ferroelectric effect [20], and anti-ferroelectric liquid crystals [21]. The maximum contrast of the input phase visualization by nonlinear Zernike system takes place at $\Delta\Phi = \pi/2$, which corresponds to the angle $\Theta = \pi/4 = 45^{o}$.

2. EXPERIMENT.

The scheme of the non-linear Zernike filter with FLC OASLM is shown in Fig. 5.

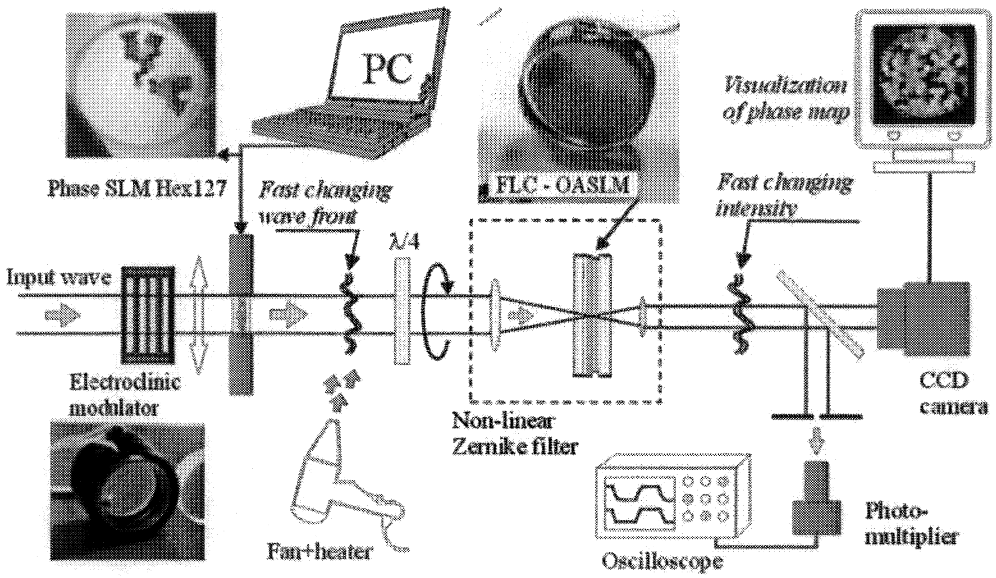

Fig.5. Setup for optical phase distortion visualization and measurements of phase shift dynamics.

2.1. OASLM.

The OASLM has a sandwich structure, composed by photo-conducting amorphous hydrogenited silicon carbide film a-SiC:H, with thickness 1μm (manufactured by PeterLab., Ltd, Russia) and a planar aligned ferroelectric liquid crystal layer with material FLC-517, developed at ARL's Intelligent Optics Lab. The FLC has a switchable molecular tilt angle of +/-22.5^o, refractive index anisotropy $\Delta n = 0.18$ (for $\lambda = 633$nm) and helix pitch of about 0.3μm. The thickness of the FLC layer is 2 μm, providing the condition of "half wavelength phase shift" for a totally untwisted state, corresponding to voltage above +/-2.5V. In the untwisted state the director of the FLC layer (direction of long molecular axes) is in the plane parallel to the electrode surface. Changing the applied voltage polarity results in a 45^o director switch. For smaller voltages the LC material operates in the DHF mode, providing gray scale deviation of optical axis in the range of about 40^o for voltages from –2V to +2V.

When the angle between the FLC directors is 45^o a phase shift of $\pi/2$ occurs only some time after polarity switching for the square wave voltage applied to the OASLM. This time depends on voltage amplitude and light beam intensity. The appearance of the $\pi/2$ phase shift is related to the difference in switching times in the areas of high and low light intensities. The intensity of light is much higher in focus resulting in actual amplitude of voltage applied to FLC in the area of focus is significantly larger than in ambient area and hence the FLC director switches faster in the area of focus. For typical input light powers near 100nW and aperture diameter 15mm the light intensity in the zero order focal spot is near 5-10mW/cm^2. This is a relatively high intensity for the amorphous silicon a-Si:H FLC OASLM [22] and the amorphous silicon carbide a-SiC:H [23] films. For applied voltages of amplitude +/-10V and input power about 100nW the switching time in the focal spot is of the order of tens of μs. In ambient area the switching process takes milliseconds due to the smaller light intensities. As a result, the difference of 45^o in orientation of the FLC director between focal spot and the ambient area remains about hundred microseconds, until the director in the ambient areas of the OASLM respond to the lower voltage produced in weakly illuminated areas. The optical state of the FLC layer shown in Fig.4b can be "frozen" by rapidly changing the external voltage polarity while the director in low intensity areas remains unchanged. The best contrast of phase visualization can be obtained if characteristic frequencies of voltage applied to OASLM are of the order of kHz.

2.2. Visualization of optical phase distortions.

Calibrated phase distortions were introduced with a multi-pixel liquid crystal optical phase modulator "Hex127" from Meadowlark Optics, Inc. Visualization of the optical phase map is shown in Fig.6 for the input light intensity near 10 nano-Watt. It was found that image contrast does not depend on rotation of the OASLM around optical axes. Regardless of the rotation angle the phase shift value is determined only by the mutual angle between the FLC director in the focal spot and in the ambient area.

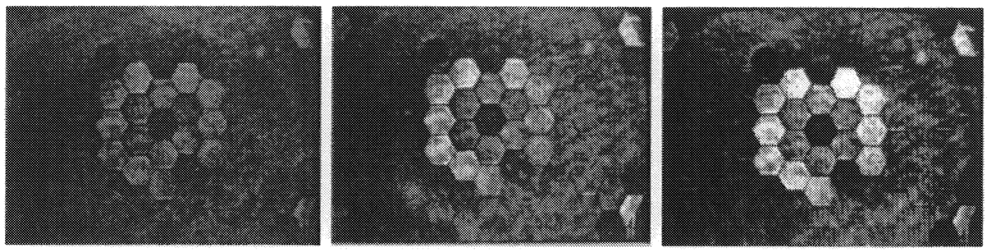

17nW 29nW 45nW

Fig.6. Visualization of SLM Hex127 phase map observed in the nonlinear Zernike filter with FCL OASLM for different input light power. The maximum amplitude of phase modulation on the SLM aperture is half wavelength.

2.3 Dynamical response of FLC OASLM based wave-front sensor.

To estimate the response time of the wave front sensor a fast multi-pixel phase SLM was designed using dual frequency nematic liquid crystal. The phase change at each pixel was in the range of 0.5-1.6 ms. The sensor's output image corresponding to the pixel location was projected onto the photo-multiplier shown in Fig. 5. The characteristic time response of the FLC Zernike filter can be estimated from the sequences of piston type phase pulses recorded using dual frequency SLM placed between crossed polarizers rotated at 45° to the LC director (Fig. 7b), and from the output nonlinear Zernike filter intensity modulation registered by photo-multiplier in Fig. 7a. As can be seen the wave front sensor is capable of reproducing optical phase pulses with rise/decay times about 0.5ms.

a

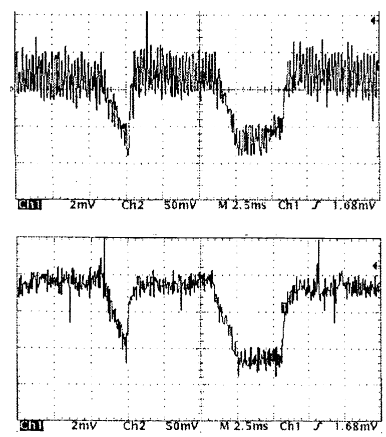

b

Fig.7. a) signal from photo-multiplier for selected pixel of the dual frequency SLM. b) signal from photo-multiplier for the same pixel placed between crossed polarizers. Frequency of square wave voltage 4kHz, +/-10V, power of input beam about 2μW.

Note that for the time diagram in Fig.7a there are no polarizing elements and modulation of intensity in photo-multiplier aperture is related only with phase visualization.

2.4. Influence of circular polarization handedness on phase visualization contrast. Differential Zernike filter.

Images of phase maps corresponding to input beam left and right circular polarizations are shown in Fig. 8 for phase patterns generated by the Hex127. As seen from the Fig. 8 the change of circular polarization handedness results in output image contrast inversion.

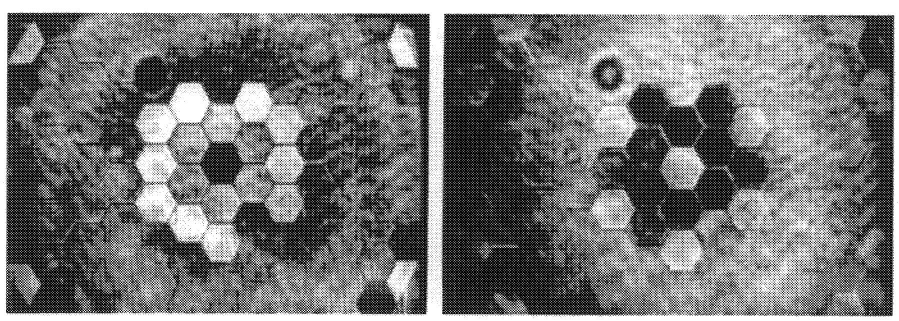

a b

Fig.8. Photos a) and b) correspond to two different orientations of λ/4 wave plate placed in front of the nonlinear Zernike sensor: a) -45° and b) +45°. Input wave power was 550nW, frequency of square wave voltage 6kHz, amplitude +/-10V, d. c. offset +1.5V.

This property of the wave sensor can be used to design the differential Zernike filter described in [15] allowing significant improvement in the sensor's contrast by subtracting two images corresponding to right and left polarization handedness.

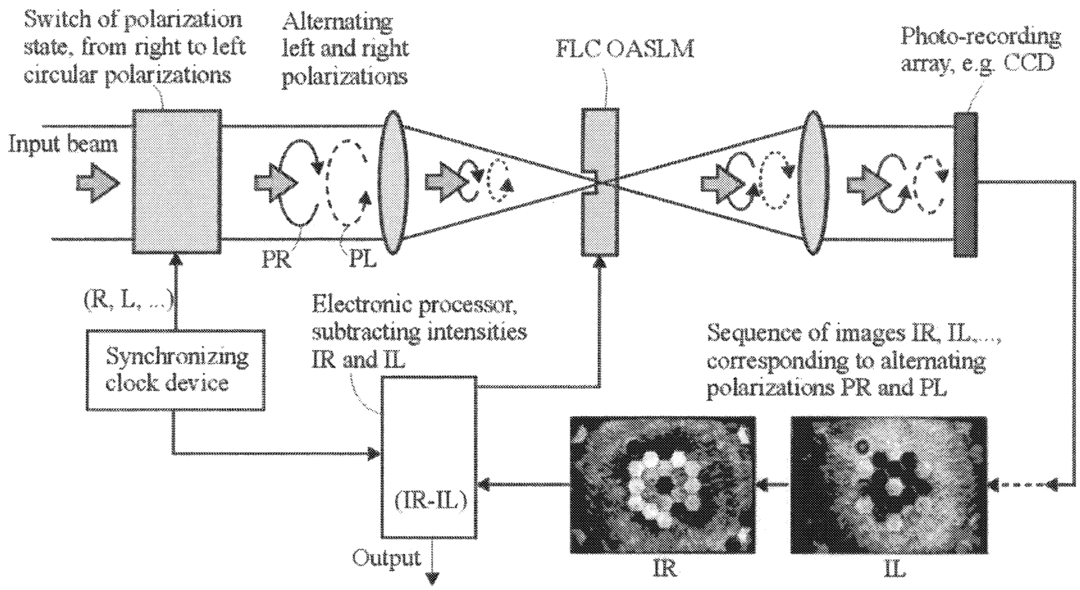

Fig.9. Block-diagram of the differential Zernike filter, using FLC OASLM.

The scheme of possible realization of the differential Zernike filter is shown in Fig. 9. An input wave passes through the polarization state switch transforming input light into one of two circular polarization states. This switch can be implemented using a combination of a linear polarizer and optical quarter wave retardation plate "$\lambda/4$ plate" that can be mechanically rotated on 90^o. Another solution is to use a LC electro-optical modulator changing from left to right circular polarization states by applying a corresponding electrical signal. The polarization switch can be build using ferroelectric liquid crystal in planar orientation similar to that used in the OASLM. The thickness of the FLC layer in such a polarization switch should correspond to quarter wavelength optical retardation. Two positions of optical axes corresponding to the orientation change of 90^o can be realized using FLC material with molecular tilt angle 45^o. Using an external control signal the FLC director can change its orientation from -45^o to $+45^o$ resulting in a switch between the two circular polarization states.
The polarization switch is synchronized with the imaging camera registering a sequence of positive and negative wavefront sensor output images. Subtraction of these images creates the differential Zernike sensor output.

2.5. Synchronization of light with voltage polarity.

We have found that contrast of the nonlinear Zernike filter based on FLC OASLM can be improved if the OASLM is illuminated during only half period of the applied square-wave (meander) voltage. The synchronization of input light pulses of a certain polarity was accomplished using a double electro-clinic modulator [24], manufactured in the ARL's Intelligent Optics Lab. The characteristic response time of the modulator was about 25 μs.
As seen in Fig.10 the best contrast was achieved when illuminating the OASLM during the half period of time corresponding to +5V amplitude of the meander voltage ranging from +5V to –10V. The contrast of the resulting image can be reversed if light pulses correspond to negative polarity of the square wave voltage with a simultaneous change of DC offset, so that light pulses correspond to –5V and no light state corresponds to +10V.

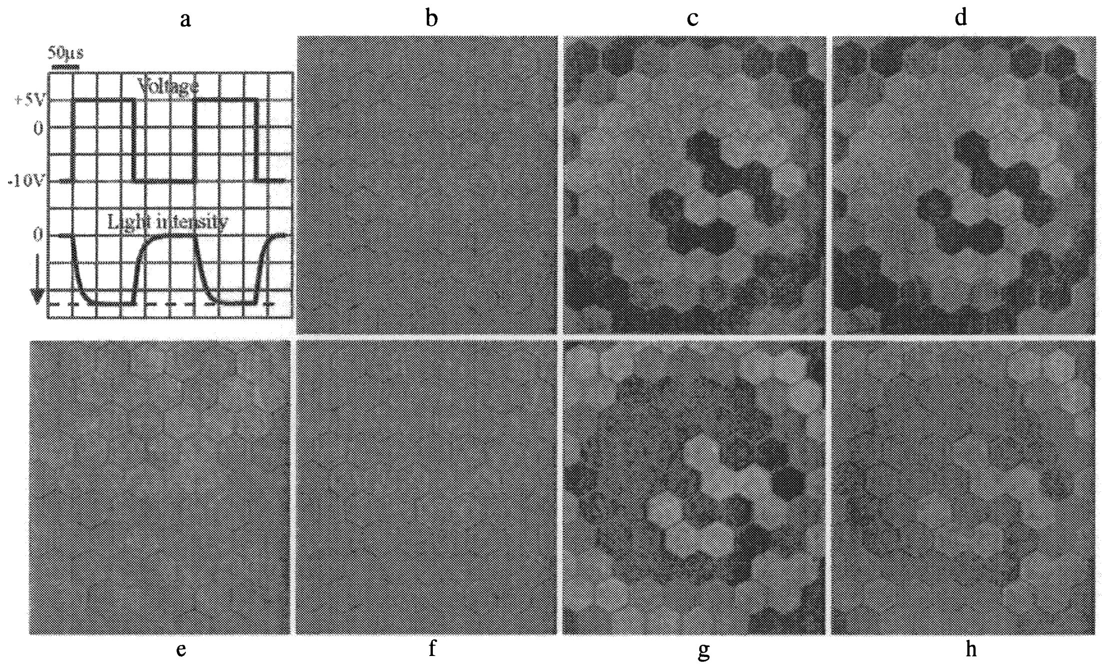

Fig.10. The influence of synchronization of voltage polarity with light pulses on output intensity contrast: a) applied to FLC OASLM 4kHz meander voltage and light pulses, b), c), d) – light pulses synchronized with positive polarity; b) applied voltage with amplitude ranged from +10 to -5V; c) from +5 to -10V, d) from +5 to -10V (c) and d) - different area of the FL OASLM was illuminated); e) no voltage applied to the OASLM, f), g), h) - light pulses are synchronized with negative polarity. f) applied voltage with amplitude ranged from +5 to -10V, g) from +10 to -5V, and h) from +10 to -5V (g) and h) - different area of the FL OASLM was illuminated).

The preferable synchronization mode corresponds to OASLM illumination when a small positive voltage is applied to the ITO electrode connected with the FLC and the dark state corresponds to a larger negative voltage applied to this electrode (Figs.10c and 10d). In this case the sensitivity of wave front sensor doesn't depend on the FLC OASLM illuminated area. Sensitivity of the wave front sensor depends on applied voltage parameters. The highest sensitivity on the order of units of nano-Watts was obtained for meander voltages ranging from +5 to -10V with repetition rate 1-2kHz and illumination at positive polarity.

A high sensitivity of the sensor to small phase distortions is illustrated in Fig.11 where visualization of small amplitude phase defects in a polymer film with thickness about 0.1μm are shown. The phase defect in Fig. 11 corresponds to less than one tenth of a wavelength.

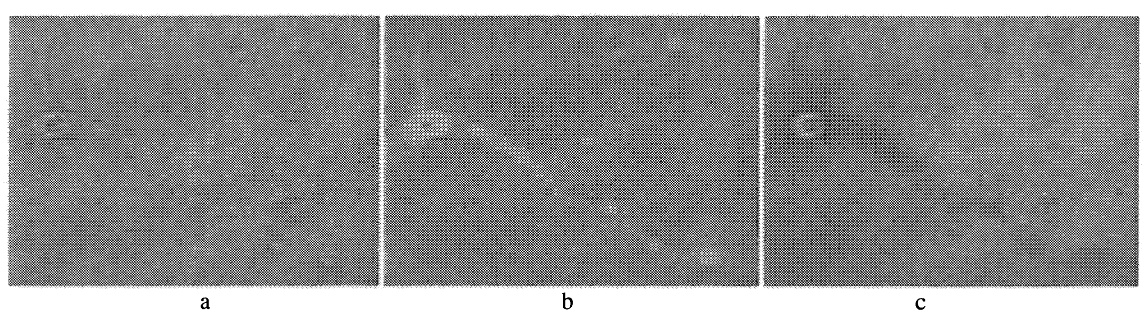

Fig.11. Visualization of phase defects in thin poly-vinyl alcohol film with thickness 0.1μm, using FLC OASLM Zernike filter. a) OASLM is OFF, b),c) OASLM is ON, +/- 10V, 4kHz, d.c. offset =2V. b) left circular polarization of input light, c) right circular polarization of input light. The picture size is 10x15mm.

2.6. Visualization of dynamical phase distortions.

Dynamical optical phase distortions were generated using the air fan and heater shown in Fig.5. The wavefront sensor output intensities corresponding to these phase distortions are presented in Fig.12.

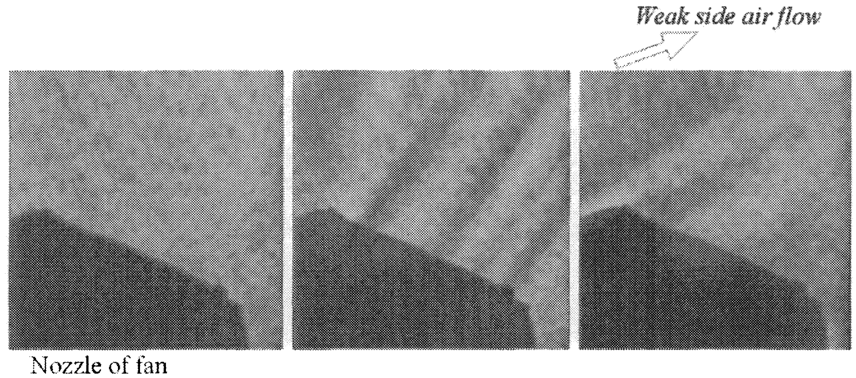

a b c

Fig.12. Visualization of weak air flows from heating fan using FLC OASLM Zernike filter.
a) OASLM is OFF, b),c) OASLM is ON.

To estimate the sensor's time response fast optical phase distortions were generated using a heating gun. A photo-multiplier placed instead of the CCD video camera (Fig. 5) was used to record dynamical changes in the sensor's output intensity.

Curves in Fig. 13 demonstrate the photo-multiplier output vs. time. If the heating gun is turned off (Fig.13 a) only the modulation with frequency 6kHz is visible. This modulation is related with small deviations of the FLC director under an applied voltage. The presence of fast changing turbulent air flows (the heating gun is on) is clearly seen in the output signal of the nonlinear Zernike filter based on FLC OASLM (Fig. 13 b). For comparison the same experiment was performed with the nonlinear Zernike filter based on nematic LC OASLM (Fig. 13 c) described in [15], see Fig.2. As seen from this output intensity evolution curve the nematic-based sensor was able to record only slowly changing components of the output intensity.

a
b
c
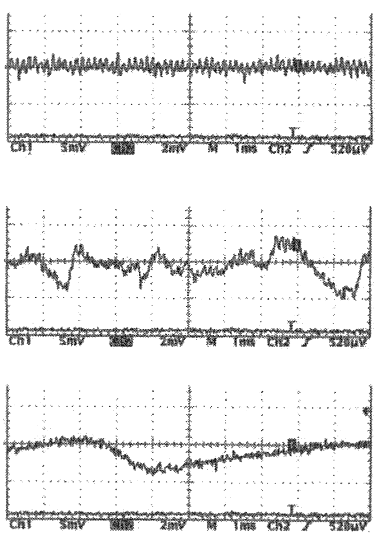

Fig.13. Oscillograms of sensor's output intensity recorded with the use of 1mm pinhole placed in front of the photo-multiplier for air turbulence generated by a heating gun:
a) Signal from FLC OASLM based wave front sensor without heater and fan. Applied meander voltage amplitudes ranged from +10V to -10V, frequency 6kHz, input light power 50nW.
b) Fan is ON. Signal recorded with ferroelectric liquid crystal OASLM;
c) Fan is ON. Signal recorded with nematic liquid crystal based OASLM. Sine wave voltage with amplitude 6V and frequency120Hz, power of the input light 0.45μW.

The time resolution of the FLC OASLM based wavefront sensor is near 200μs. The nematic liquid crystal based OASLM allows resolution of optical phase distortions within the range of 2-3ms.

3. CONCLUSIONS

A wave front sensor based on a non-linear Zernike filter utilizing an optically addressed spatial light modulator is described. The sensor is based on FLC OASLM composed by ferroelectric liquid crystalline and amorphous hydrogenited silicon carbide films. The sensor has high light sensitivity (on the order of tens of nanoWatts) and the response time is on the order of 200μs. We also discussed the differential Zernike filter architecture based on switchable FLC optical $\lambda/4$ retardation plate.

REFERENCES

1. J. W. Hardy, J. E. Lefebvre, and C. L. Koliopoulos, "Real-time atmospheric compensations", ***J. Opt. Soc. Am.* 67**, pp.360-369, 1977.
2. D. G. Sandler, L. Guellar, M. Lefebvre, T. Barrett, R. Arnold, P. Johnson, A. Rego, G. Smith, B. Taylor, and G. Spiv, "Shearing interferometry for laser-guide-star atmospheric correction at large D/r_0", ***J. Opt. Soc. Am. A* 11**, pp. 858-873, 1994.
3. J. W. Hardy, "Active optics: a new technology for the control of light", ***Proc. IEEE***, **66**, pp. 651-697, 1978.
4. F. Roddier, "Curvature sensing and compensation: a new concept in adaptive optics", ***Appl. Opt.***, **27**, pp. 1223-1225, 1988.
5. G. Rousset, "Wavefront sensors", in ***Adaptive Optics in Astronomy***, ed. F. Roddier, Cambridge U. Press, New York, 1999, pp. 91-130.
6. M. C. Roggemann and B. Welsh, ***Imaging through Turbulence***, CRC Press, Boca Raton, Fla., 1995.
7. R. W. Gerchberg and W. O. Saxon, "A practical algorithm for the determination of phase from image and diffraction plane pictures", ***Optik***, **35**, pp. 237-246, 1972.
8. J. R. Fienup, "Phase retrieval algorithm: a comparison", ***Appl. Opt.***, **21**, pp.2758-2769, 1982.
9. V. Yu. Ivanov, V. P. Sivokon, and M. A. Vorontsov, "Phase retrieval from a set of intensity measurements: theory and experiment", ***J. Opt. Soc. Am. A* 9**, pp. 1515-1524, 1992.
10. R. A. Gonsales, "Phase retrieval from modulus data", ***J. Opt. Soc. Am.* 66**, pp. 961-964, 1976.
11. R. G. Raxman and J. R. Fienup, "Optical misalignment sensing and image reconstruction using phase diversity", ***J. Opt. Soc. Am. A* 5**, pp. 914-923, 1988.
12. J. W. Goodman, ***Introduction to Fourier Optics***, McGraw-Hill, New York, 1996.
13. S. A. Akhmanov and S. Yu. Nikitin, ***Physical Optics***, Claredon, Oxford, UK, 1997.
14. F. Zernike, "How I discovered phase contrast", ***Science,*** **121**, pp.35-349, 1955.
15. M. A. Vorontsov, E. W. Just, and L. A. Beresnev, "Adaptive Optics with Advanced Phase-Contrast Techniques. Part I. High-Resolution Wavefront Sensing", ***J. Opt. Soc. Am. A.***, **18**, 2001.
16. E. W. Just, M. A. Vorontsov, G: W: Carhart, and L. A. Beresnev, "Adaptive Optics with Advanced Phase-Contrast Techniques. Part II. High-Resolution Wavefront Control", ***J. Opt. Soc. Am. A.***, **18**, 2001.
17. M. Martinelli and P. Vavassori, "A geometric (Pancharatnam) phase approach to the polarization and phase control in the coherent optics circuits", ***Optics Communications,*** **80**, pp.166-176, 1990; J. E. Stockley, G. D. Sharp, S. A. Serati and K. M. Johnson, "Analog optical phase modulator based on chiral smectic and polymer cholesteric liquid crystal", ***Optics Letters***, **20**, pp. 2441-2443, 1995; ", ***US Patent 5,381,253***.
18. N. A. Clark and S. T. Lagerwall, "Submicrosecond bistable electro-optic switching in liquid crystals", ***Appl. Phys. Lett.***, **36**, pp.899-901, 1980; ***US Patents 4,813,767, 4,563,059.***
19. S. Garoff, and R. B. Meyer, "Electroclinic Effect at the A-C Phase Change in a Chiral Smectic Liquid Crystal", ***Phys. Rev. Lett.***, **38**, pp.848-851; S. T. Lagerwall, G. Andersson, I. Dahl, W. Kuczynski, K. Skarp, and B. Stebler, ***US Patent 4,838,663***.
20. L. A. Beresnev, V. G. Chigrinov, D. I. Dergachev, E. P. Pozhidayev, J. Fünfschilling, and M. Schadt, "Deformed helix ferroelectric liquid crystal display: A new electrooptical mode in ferroelectric chiral smectic C liquid crystals", ***Liquid Crystals***, **5**, 1171-1177 (1989); ***US Patents 5,770,109, 5,676,880***.
21. A. D. L. Chandani, T. Hagiwara, Y. Suzuki, Y. Ouchi, H. Takezoe and A. Fukuda, "Tristable Switching in Surface Stabilized Ferroelectric Liquid Crystals with a Large Spontaneous Polarization", ***Jpn J. Appl. Phys.***, **27**, L729-L732, 1988; A. Fukuda, Y. Takanishi, T. Isozaki, K. Ishikawa and H. Takezoe, "Antiferroelectric Chiral Smectic Liquid Crystals", ***J. Mater. Chem.***, **4**, pp.997-1016, 1994.
22. I. Abdulhalim, G. Moddel, and K. M. Johnson, "High-speed analog spatial light modulator using a hydrogenited amorphous silicon photosensor and an electroclinic liquid crystal", ***Appl. Phys. Lett.***, **55**, pp.1603-1605, 1989; Abdulhalim, B. Landreth, G. Moddel, "Analog Optically Addressed Spatial Light Modulator with Pseudocolor Capability Using Helix Distortion of Ferroelectric Liquid Crystal", ***SID 90 Digest***, pp.330-333, 1990; S. Fukushima, T. Kurokawa, S. Matsuo, H. Kozawaguchi, "Bistable spatial light modulator using a ferroelectric liquid crystal", ***Optics Letters***, **15**, pp.285-287, 1990.
23. K. Akijama, A. Takimoto, and H. Ogawa, "Photoaddressed spatial light modulator using transmissive and highly photosensitive amorphous-silicon carbide film", ***Applied Optics***, **32**, pp.6493-6500, 1993.
24. L. A. Beresnev and W. Haase, "Ferroelectric liquid crystals – development of materials and fast electrooptical elements for non-display applications", ***Optical Materials***, **9**, pp.201-211, 1998.